Journal of Engineering Science and Technology
Vol. 16, No. 2 (2021) 988 - 1005

DESIGN AND ANALYSIS OF MULTI-FINGER ROBOTIC HAND

ENASS H. FLAIEH[1,*], HAIDER G. KAMIL[2, 3],
SADEQ H. BAKHY[1],MORTADA A. JABBAR[1]

[1]Mechanical Engineering Department, University of Technology- Iraq, Baghdad, Iraq
[2]Electrical & Electronic Engineering Department, College of Engineering, University of Kerbala/ Kerbala, Iraq
[3]Department of Computer Engineering Techniques, AlSafwa University College/ Kerbala, Iraq
*Corresponding Author: enass.h.flaieh@uotechnology.edu.iq

Abstract

Grasping and manipulation tasks are the main objective of the development of robotic hands. In particular, the under actuation in grasping is to use an ingenious mechanical system that can adapt to the shape of the object automatically. Recent studies have highlighted the need to increase the mechanical advantages of these systems. In this paper, a transmission ratio of the underactuated linkage robotic finger has been formulated using finger geometric parameters, where the performance of the linkage-driven three-phalanx fingers has been dictated by the ratio of the output link to the input link lengths of the four-bar linkage mechanism. The proposed design and fabrication of a multi-finger robotic hand mechanism with three articulated fingers are being developed. The finger consists of two-four bar linkages, links in series. A DC motor has been attached to the coupler link of the second phalanx of each robotic finger. Thus, the link length has been adjusted to reach the required length to perform either grasping or pinching configurations. A single actuator has been used to accelerate the whole hand mechanism. The Proportional, Integral, and Derivative (PID) control technique has been utilized to control grasping and pinching objects. Experimental results show the success of controlling the robotic hand movement and complete the required purpose.

Keywords: Four-bar linkage, Grasping, Pinching, Transmission ratio, Under-actuated robotic hands.

1. Introduction

One of the most exciting fields in the robotic hand's design is the underactuated robotic hand concept, which was proposed by Gosselin and his co-workers at Laval University, Canada. The underactuated robotic hands possess fewer actuators than the degrees of freedom number. A reduction of actuators means less weight, fewer costs, and a more robust hand [1]. The purpose of it is to get a robotic hand able to mimic the essential tasks of the human fingers [2, 3]. In fact, in the underactuated systems, the robotic fingers use the combination of active and passive joints to provide synchronous joints movement, which is one of the significant lineaments of the human fingers [4, 5].

Many research papers have been focused on underactuated robotic hands. For an instant, a hand has three symmetrical fingers called Delft Hand II, proposed by Meijneke et al. [6]. The hand had 6 degrees of freedom and a single actuator without sensors. The motor torque was distributed among the fingers using a differential mechanism. Every finger is comprised of 2 phalanges motivated via a four-bar linkage mechanism.

The input motor voltage is used to control the contact forces. Grasping method to pick the specific region of objects introduced by Maximo A. Roa et al. [7], the region was reached using the object local curvature to determine the initial opposing grasp either two or three fingers. The points contact was dependent on the simulation and the force property. The database was collected according to the force closure grasps, which is applied to the objects. Sample objects were chosen to specify the best location for grasping objects, assumed the models of hand and object are available.

Atzori et al. [8] presented a study of electromyography data for non-invasive prostheses robotic hand. Improved and experiment with movement recognition, and the algorithms of force control were the aim of that paper. The objective was to study the relationship between surface electromyography, hand kinematics, and kinetic analysis. The study verified that the data were similar to the data that was in real condition; thus, the recognition of different hand operations by applying the signal features and machine learning algorithms was possible.

Marcenko [9] introduced an anthropomorphic manipulator with four fingers; the proposed manipulator was capable of fitting into the commercial category of prosthetics. The robotic hand was able to effectively secure most of the grips/pinches and making the needed processes without severe restrictions of the absence of the (5th) finger. The suggested manipulator was capable of resisting the force of (10 N) at each fingertip at the same time and was significantly resistant to stress; thus, it is appropriate for the industrial uses.

Wu Licheng et al. [10] proposed a new kind of totally rotating joint linkage-based underactuated mechanism, a new technique based upon the minimum resistance law was introduced for realizing the corresponding mechanism at various conditions of finger contact, the kinematic analysis based upon the corresponding mechanism. Also, the kinematic equations and the limit moving the location of the mechanism were derived utilizing the suggested technique. Numerical simulation was conducted using MATLAB software. The accuracy and efficiency of the suggested technique were confirmed. The results of the

simulation showed that the suggested mechanism had a significant grasp space and can perform a good grasp trajectory.

Ha and Nguyen [11] developed a mathematical analysis of contact forces for an underactuated finger in a universal underactuated robotic hand throughout the grasping action. Due to the significance of contact force, the suggested technique for static analysis of the contact force is focused on the (n-DOF) underactuated finger. The results of the simulation, with the (3-DOF) underactuated finger from the (ADAMS) model, showed the efficiency of the mathematical analysis technique and compared the measured outcomes with, particularly, the steadiness and convergence in control use. The regime could obtain the contact force magnitudes at the contact positions between the finger phalanges with the object.

Carbone et al. [12] introduced a pair of robotic hands developed at the University Federico II of Naples, and at the University of Cassino, FEDERICA Hand and LARM Hand were characterized with respect to design and working aspects. Considerable care was given to the dissimilarities between the aforementioned hands with respect to the systems of transmission. FEDERICA Hand used pulleys and tendons for driving the phalanxes, whereas LARM Hand utilized cross 4-bar linkages. The results of experimental tests were documented to reveal how the main design topics influence the performance of every robotic hand.

Zappatore et al. [13] presented a software framework for helping a user throughout the design period of a humanoid robotic hand that utilized underactuated fingers toward the optimization of grasp steadiness. The tool was more parameterized to manage with different parameters that contain the thickness and length of the phalanx, driving torque, properties of joint spring, and friction.

Though it was mainly planned for parametric design of a humanoid underactuated hand utilizing the simulated grasping, it could also be worth as an educational tool for helping the non-expert employers or students to recognize the principles that underlie the underactuated grasp via visualizing in what way the parameter slides bars effect upon the indexes of steadiness.

However, this paper attempts to suggest a new formulation of the transmission ratio of the output torque to the input torque of the robotic finger, to determine the hand parameters (transmission mechanisms links lengths), such that they can be physically implemented in an underactuated mechanism. The proposed design of a robotic hand with three underactuated fingers, to achieve human hand configuration during grasping and pinching, based on a four-bar linkage mechanism to provide relatively high grasping and pinching forces, was introduced. Finally, the robotic hand has been tested for both configurations, and the experimental results were debated

2. Design Guidelines

The underactuated robotic hand's performance is obtained via the dimensional finger design, the palm, and the finger actuation mechanism. The actuation system function is to spread the torque of the actuator to the phalanges of the finger at the desired ratio (R). R is defined by the torque exerted to the distal phalanx (T_1) divided by the torque exerted to the proximal phalanx (T_2) [14, 15]:

$$R = \frac{T_2}{T_1} = \frac{\omega_1}{\omega_2} \quad (1)$$

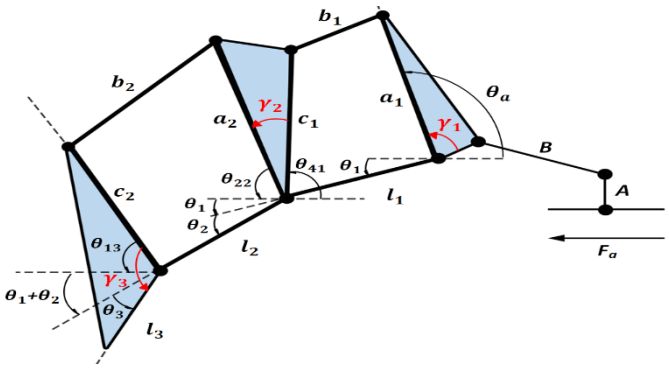

Fig. 1. Geometric parameters of the three degrees of freedom under the actuated robotic finger.

Referring to Figs. 1, 2(a), and 2(b) for the first four-bar linkage.

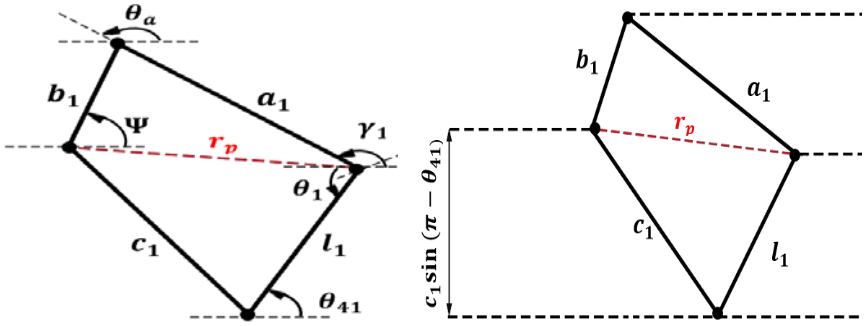

(a) Geometric parameters of the 1st four-bar linkage.

(b) Calculating sine and cosine of angle Ψ.

Fig. 2. Geometric parameters of the first four- bar linkage.

According to the law of cosine.

$$r_p^2 = a_1^2 + b_1^2 - 2a_1 b_1 cos\,(\theta_a - \Psi) \quad (2)$$

$$r_p^2 = c_1^2 + l_1^2 - 2c_1 l_1 cos\,(\theta_{41} - \theta_1) \quad (3)$$

Equating Eqs. (2) and (3).

$$a_1^2 + b_1^2 - 2a_1 b_1 cos\,(\theta_a - \Psi) = c_1^2 + l_1^2 - 2c_1 l_1 cos\,(\theta_{41} - \theta_1) \quad (4)$$

To find the angle Ψ;

$$sin\Psi = \frac{l_1 sin\theta_1 + a_1 sin(\pi - \theta_a) - c_1 \sin(\pi - \theta_{41})}{b_1} \quad (5)$$

$$cos\Psi = \frac{l_1 cos\theta_1 + c_1 cos(\pi - \theta_{41}) - a_1 \cos(\pi - \theta_a)}{b_1} \quad (6)$$

Substitute Eqs. (5) and (6) in Eq. (4) moreover, simplifying.

$$b_1^2 - a_1^2 - 2a_1l_1cos\theta_1cos\theta_a + 2a_1c_1cos\theta_{41}cos\theta_a - 2a_1l_1sin\theta_asin\theta_1 + 2a_1c_1sin\theta_{41}sin\theta_a = c_1^2 + l_1^2 - 2c_1l_1cos\theta_{41}cos\theta_1 - 2c_1l_1sin\theta_{41}sin\theta_1 \quad (7)$$

Deferential of Eq. (7) concerning time for a specified configuration that θ_1 , θ_2 *and* θ_3 will be constant, the transmission ratio depends only on the input and output velocities of the four-bar linkage mechanisms. Notice that $\dot{\theta_a} = \omega_a$ & $\dot{\theta_{41}} = \omega_{41}$, then

$$\omega_a(2a_1l_1cos\theta_1sin\theta_a - 2a_1c_1sin\theta_acos\theta_{41} - 2a_1l_1sin\theta_1cos\theta_a + 2a_1c_1sin\theta_{41}cos\theta_a) + \omega_{41}(-2a_1c_1sin\theta_{41}cos\theta_a + 2a_1c_1sin\theta_acos\theta_{41} - 2c_1l_1sin\theta_{41}cos\theta_1 + 2c_1l_1sin\theta_1cos\theta_{41}) = 0 \quad (8)$$

According to Fig. 3, for the second four-bar linkage, using cosine law:

$$r_p^2 = l_2^2 + c_2^2 - 2l_2c_2cos\ (\theta_{42} - \theta_1 - \theta_2 \quad (9)$$

$$r_p^2 = a_2^2 + b_2^2 - 2a_2b_2cos\ (\theta_{22} - \Psi_1 \quad (10)$$

Equating Eqs. (9) and (10)

$$l_2^2 + c_2^2 - 2l_2c_2cos\ (\theta_{42} - \theta_1 - \theta_2)\ = a_2^2 + b_2^2 - 2a_2b_2cos\ (\theta_{22} - \Psi_1) \quad (11)$$

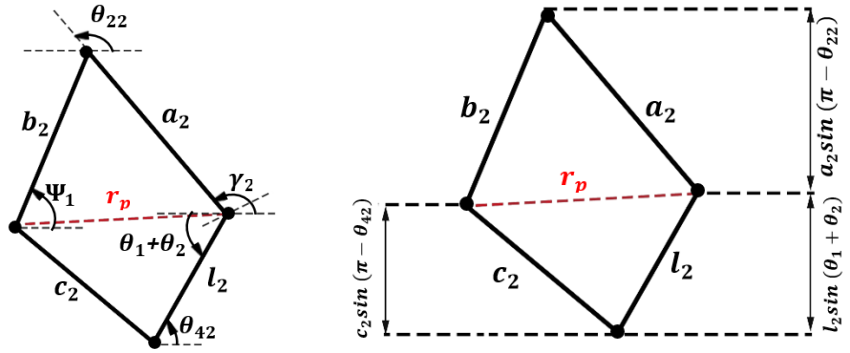

(a) Geometric parameters of the 2nd four-bar linkage. **(b) Calculating sine and cosine of the angle Ψ_1.**

Fig. 3. Geometric parameters of the second four- bar linkage.

To find $sin\Psi_1$, *and* $cos\ \Psi_1$,

$$sin\Psi_1 = \frac{a_2sin\ (\pi-\theta_{22}) + l_2sin\ (\theta_1+\theta_2) - c_2sin\ (\pi-\theta_{42})}{b_2} \quad (12)$$

$$cos\Psi_1 = \frac{l_2cos\ (\theta_1+\theta_2) - a_2cos\ (\pi-\theta_{22}) + c_2cos\ (\pi-\theta_{42})}{b_2} \quad (13)$$

Substitute Eqs. (12) and (13) in Eq. (11) moreover, simplifying.

$$l_2^2 + c_2^2 - 2l_2c_2(cos\theta_{42}cos(\theta_1 + \theta_2) + sin\theta_{42}sin(\theta_1 + \theta_2)) =$$

$$a_2^2 + b_2^2 - 2a_2[l_2cos\theta_{22}cos\ (\theta_1 + \theta_2) - c_2cos\theta_{42}cos\theta_{22} + l_2sin\theta_{22}sin\ (\theta_1 + \theta_2) - c_2sin\theta_{42}sin\theta_{22}] \quad (14)$$

Differential concerning time; were, $\dot{\theta_{22}} = \omega_{22}$ & $\dot{\theta_{42}} = \omega_{42}$, then:

$$\omega_{42}[2l_2c_2cos\ (\theta_1+\theta_2)\ sin\ \theta_{42}-2l_2c_2cos\ \theta_{42}sin\ (\theta_1+\theta_2)+2a_2c_2sin\theta_{42}cos\theta_{22}-2a_2c_2sin\theta_{22}cos\theta_{42}]+\omega_{22}[-2a_2l_2sin\theta_{22}cos\ (\theta_1+\theta_2)+2a_2c_2cos\theta_{42}sin\theta_{22}-2a_2c_2sin\theta_{42}cos\theta_{22}+2a_2l_2cos\theta_{22}sin\ (\theta_1+\theta_2)\ ]=0 \quad (15)$$

As the velocity of the output link of the first four-bar linkage is equal to the velocity of the input link of the second four-bar linkage, substitute Eq. (15) in Eq. (8) where $\omega_{41}=\omega_{22}$;

$$\frac{\omega_a(-2a_1l_1cos\theta_1sin\theta_a+2a_1c_1sin\theta_acos\theta_{41}+2a_1l_1sin\theta_1cos\theta_a-2a_1c_1sin\theta_{41}cos\theta_a)}{-2a_1c_1cos\ \theta_a\ sin\ \theta_{42}+2a_1c_1sin\theta_acos\theta_{41}-2c_1cl_1cos\theta_1sin\theta_{41}+2c_1l_1sin\theta_1cos\theta_{41}}=$$

$$\omega_{42}[-2c_2l_2sin\theta_{42}cos\ (\theta_1+\theta_2)+2l_2c_2cos\theta_{42}sin(\theta_1+\theta_2)-2a_2c_2sin\theta_{42}cos\theta_{22}+2a_2c_2sin\theta_{22}cos\theta_{42}]/\ (-2a_2l_2sin\theta_{22}\cos(\theta_1+\theta_2)+2a_2c_2sin\theta_{22}cos\theta_{42}+2a_2l_2\sin(\theta_1+\theta_2)\,cos\theta_{22}-2a_2c_2sin\theta_{42}cos\theta_{22})=0 \quad (16)$$

Getting eqn. between ω_a & ω_{42}, where:

$$R=\frac{\omega_a}{\omega_{42}}=\frac{Torque\ applied\ to\ the\ proximal\ phalanx}{Torque\ applied\ to\ the\ distal\ phalanx} \quad (17)$$

Simplify Eq. (16) and sub. in Eq. (17)

$$\frac{\omega_a}{\omega_{42}}=\frac{T_2}{T_1}=\frac{c_2l_2sin\ (\theta_{42}-(\theta_1+\theta_2)+a_2c_2sin(\theta_{22}-\theta_{42})}{a_1c_1sin\ (\theta_a-\theta_{41})+a_1l_1sin\ (\theta_a-\theta_1)}X\frac{a_1c_1sin\ (\theta_a-\theta_{41})+c_1l_1sin\ (\theta_1-\theta4_1)}{a_2l_2sin\ (\theta_{22}-(\theta_1+\theta_2))+a_2c_2sin(\theta_{22}-\theta_{42})} \quad (18)$$

The transmission ratio could be utilized as an optimization objective function, to be maximized to determine the dimensional design parameters of the robotic finger, to distribute the maximum torque to the three phalanges, which accordingly result in maximizing the grasping forces in the optimized underactuated robotic hand.

Referring to Eq. (18), $\theta_{22}=\theta_{41}$ in case the second four-bar linkage was directly connected to the first four-bar linkage, while $\theta_{22}=\theta_{41}+\gamma_2$, if the second four-bar linkage was connected to the first four-bar linkage via a solid ternary link. It was noticed that the transmission ratio of the robotic underactuated linkage robotic finger depends on the lengths of each four-bar linkage, where the grounded lengths represent the finger phalanges lengths within a specified range of $\theta_1, \theta_2\ and \theta_3$.

3. The Three Degrees of Freedom Fingers

The schematic diagram of the proposed modified underactuated robotic finger mechanism for the robotic hand is shown in Fig. 4(a). As illustrated in Figs. 4(b) and 4(c), each of the three fingers has three phalanges; the first and second phalanx are driven by four-bar linkages that connected in series while the third phalanx represents the output link of the second four-bar linkage.

The finger movement of the grasping assignment starts at the input link of the first four-bar linkages. As shown in Fig. 5(a), the input link will accelerate the coupler link, then the output link of the first four-bar linkage, which accelerates the first phalanx, as the first phalanx is in contact with the grasped object, the motion is transmitting to the second four-bar linkage, then the middle phalanx, as it will be in contact with the grasped object, the motion will be transmitted to the distal phalanx. Finally, all the three phalanges will be in contact with the object which

can envelop the grasped object adapting to its shape as indicated in Fig. 5(b). Referring to Fig. 5(c), a DC motor that composed of coupling and screw is attached to the coupler link of the second four-bar linkage for reducing the length of the link length to the optimized pinching length to adjust the length of the link in order to perform either the grasping or pinching configurations.

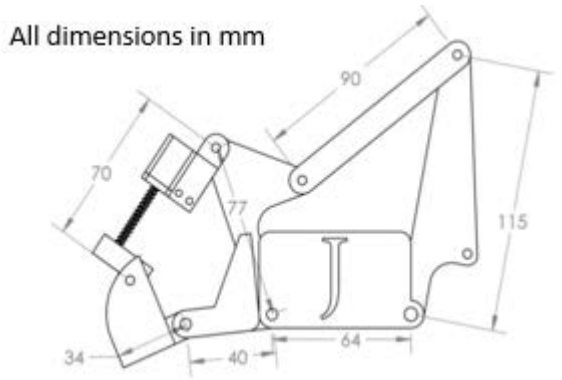

(a) Schematic diagram of the robotic finger.

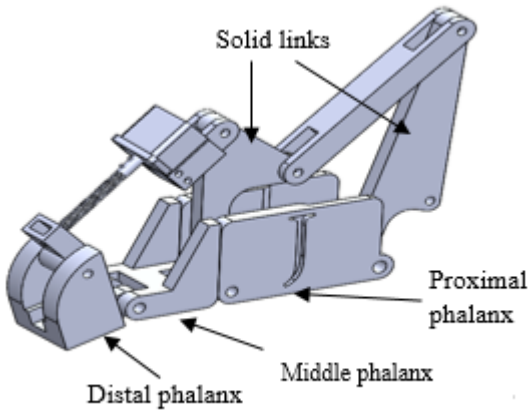

(b) Robotic finger mechanism.

(c) Picture of the robotic hand.

Fig. 4. CAD model of the underactuated robotic finger, showing its dimensions.

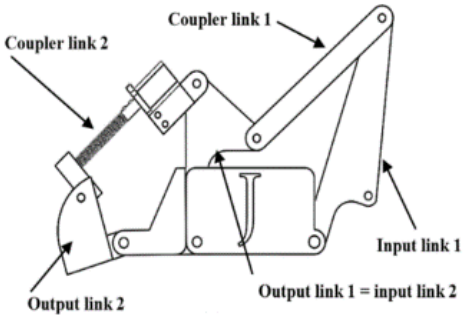

(a) Links of robotic finger.

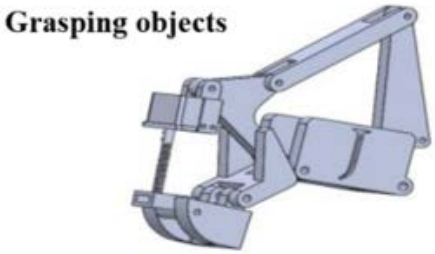

(b) Finger during graspingassignment.

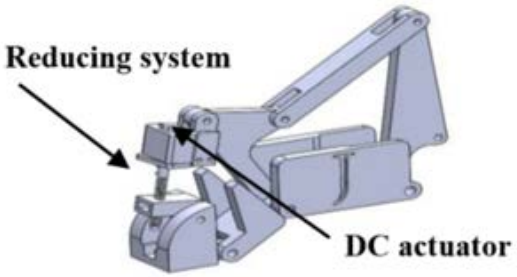

(c) Finger during pinching assignment.

Fig. 5. Robotic finger during grasping and pinching assignments.

Adding torsional springs in the passive second and third revolute joints of the robotic finger is to adjust the general geometry for grasping and pinching objects. The solid ternary links between the two sets of four-bar mechanisms for the robotic finger enable fully embrace the objects, especially small objects compared to the same finger without solid ternary links.

4. Mechanism of the Robotic Hand

The proposed hand is composed of three identical underactuated linkage robotic fingers. The fingers are arranged in two opposing one configuration in such a way

that one output must be near the sum of the other two fingers in the configuration of grasping and pinching. In pinching or secure grasping, only the fingers tips are utilized, which permits the tiny objects grasping. The hand has nine degrees of freedom, every finger has three rotational degrees of freedom.

In the power grasping mechanism, which is associated with large grasping forces, and the contact areas are located along with the hand and the phalanges enveloping the cylindrical objects [1]. The fingers have an overall length of 9.1 cm from the finger base joint to fingertip, the phalanges' lengths from the base to the tip are, 4.3 cm, 25 cm, and 23 cm respectively, which have been chosen according to the human hand characteristics. The transmission four-bar linkage lengths have been optimized employing the Gradient Descent method [16]. The robotic hand parts are made of Polylactic acid plastic material (PLA).

4.1. Palm

The hand palm is illustrated in Fig. 6, where its size estimated through a review of the robotic finger dimensions. Three identical fingers are mounted on the palm. The palm allows the fingers to move in a determined configuration to perform the required tasks. The arrangement of the fingers on the palm, as shown in Fig. 6 and A-1(*Appendix A*). There is a measured distance between the two fingers to allow the interference among the three fingers to avoid the damage that could occur to the fingers through the grasping configurations.

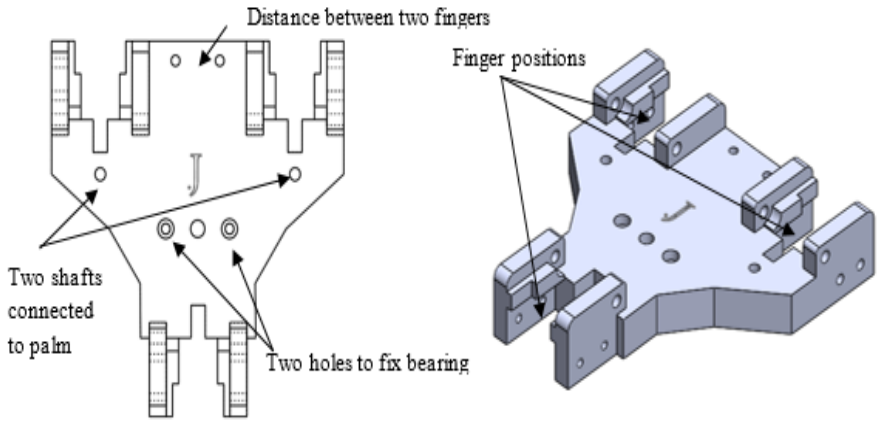

Fig. 6. Palm of the robotic hand.

4.2. Hand structure

The implemented proposed hand design is shown in Figs. 7(a) and 7(b). It is composed of the base that includes a 12V DC motor, which is one that will give the input torque to the robotic hand for accelerating the three robotic fingers together.

The multi-turn potentiometer was coupled with the DC motor via a belt to determine the actuator position instantaneously. There are two holes in the base of the robotic hand for fixing two shafts which connect the hand base to the palm of the robotic hand, which is shown in Fig. 8 The palm and the base of the robotic

hand have been connected by three bars to construct the whole hand structure. Figure. A-2 (*Appendix A*) illustrates the dimensions of the robotic hand base.

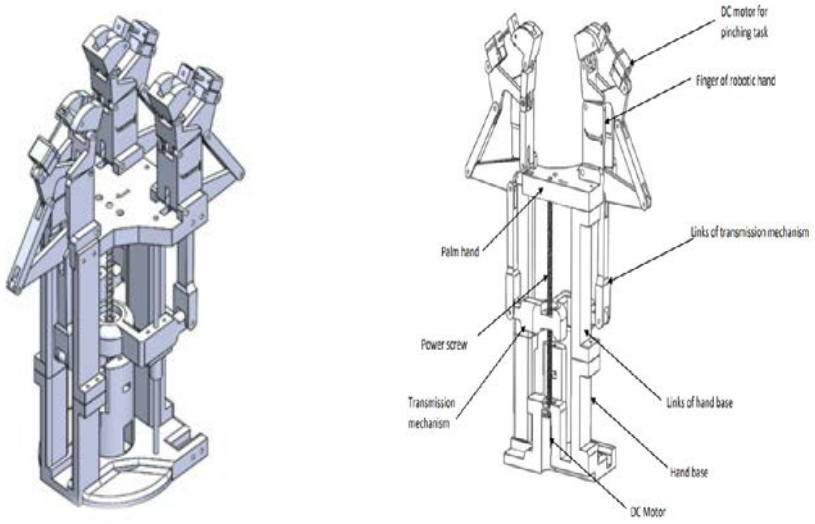

(a) CAD model of the robotic hand **(b) Section for the robotic hand**

Fig. 7. The proposed robotic hand mechanism.

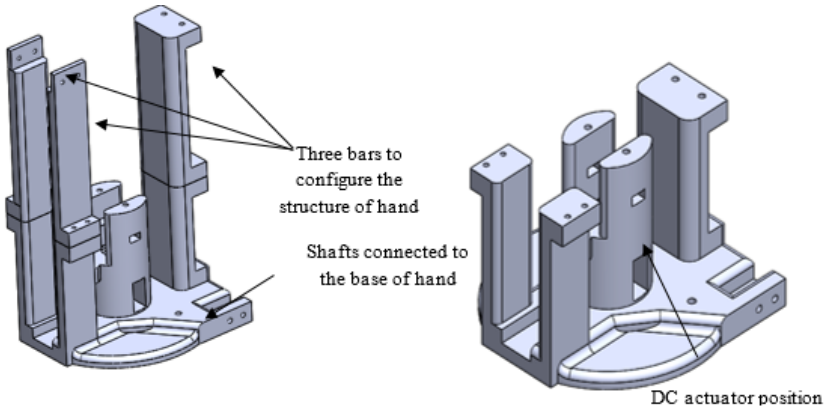

Fig. 8. Hand base mechanism of the robotic hand.

4.3. The transmission mechanism for the robotic hand

It is desired to convert the rotational motion of the input (DC) motor into a linear motion to accelerate the three fingers. The proposed mechanism composed of three bars connected, two bars connected in parallel, and the third is being opposed to them. Three links are connected with the end of each side of the mechanism. Each link is coupled to the input link of the first four-bar linkages of each finger to transmit the motion from the transmission mechanism to each finger mechanism. A screw was installed at the bottom of the palm, which was coupled to the DC motor to accelerate the transmission mechanism. The screw fixed using two linear

bearings. The linear bearing was mounted with the two circular shafts to enable the movement of the transmission mechanism and to prevent damage that may be occurred during the movement. Figure 9 presents the transmission mechanism for each finger.

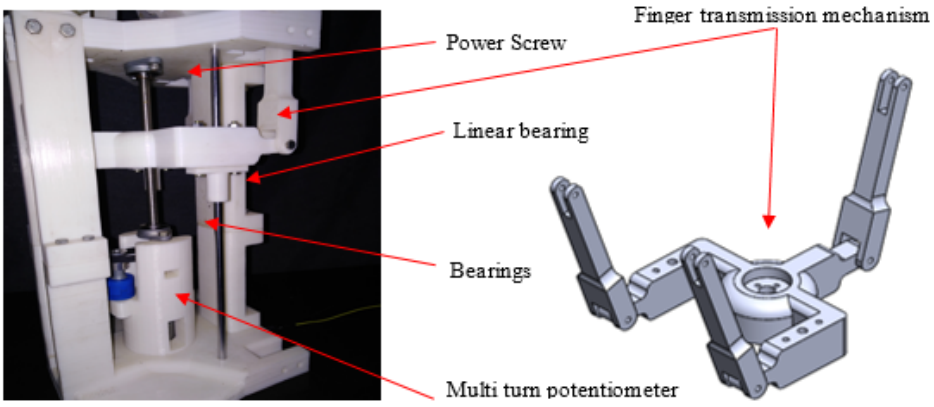

Fig. 9. Hand transmission mechanism, one input, three output.

5. Control Strategy

The control strategy was adopted to visualize the grasping and pinching configurations of the implied underactuated robotic hand. Proportional, Integral, and Derivative (PID) controller was designed to perform enveloping grasps. It is a control loop mechanism employing feedback that is widely used in industrial control systems and a variety of other applications requiring continuously modulated control. The control input to the system was the DC motor voltage signal. The control input is given as:

$$u(t) = K_p e(t) + K_i \int_0^t e(\tau)d\tau + K_d \frac{d}{d(t)}\, e(t) \tag{19}$$

where $u(t)$ is the output voltage signal of the control system, while K_p, K_i , $and\ K_d$ are proportional, Integral and Derivative constant gains that could be adjusted experimentally using trial and error realized the system experience and on the repeated experiments. The system error could be obtained by subtracted measured point at any time from the set reference point, which is determined for each object previously, written as (e), (t) is the instantaneous time. (τ) is the magnitudes from time (0) to an instantaneous (t) [17]. A multi-turn potentiometer was mounted on the actuator to determine the instantaneous position for each configuration.

Belt was used to connect the multi-turn potentiometer with the DC motor to specify the output voltage signal from the potentiometer to determine the linear hand position at any time, which played a key role in the control process. In the PID position controller. It was desired to calculate the error between the setpoint and the instantaneous point at each time. This signal gave the instantaneous position of the robotic hand to reach the predefined position, which was determined for each object Previously. The output voltage signal for the potentiometer was zero volts when the robotic hand was at zero position. The maximum linear distance for the robotic hand was 73 mm. While the maximum output voltage signal from the multi-

turn potentiometer was 5V. In order to translate the output voltage signal of the potentiometer to a linear distance, the following equation was used:

$$L = \frac{73}{5} \times multi\ potentiometer\ reading\ (volt) \quad (20)$$

where (L) is the predefined position. The PID controller is used to minimize the error until attaining the setpoint (predefined position) or less.

5.1. Experimental setup and tuning of PID parameters

Before determining the PID controller parameters, the whole control system was constructed. The Main DC motor, which accelerates the whole hand, the multi-turn potentiometer connected with the microcontroller to start the controller process. The main DC motor connected with VNH2SP30 full-bridge motor driver and linked to the microcontroller. As well as the finger's DC motors linked with L298N motor driver. PID controller constant gains were chosen empirically based on the trial-and-error method. The robotic hand was trained to grasp or pinch the selected objects and recorded the determined outputs for each object stably and securely. PID controller code was implemented using the Arduino IDE.

Initially, values of PID parameters were adjusted to zero, then increased individually and gradually until reaching the required stability of the system. The PID parameters tuned manually to $K_p = 7$, $K_i = 0.29$ and $K_d = 0.015$, where the controller used C^{++} software.

5.2. Practical test

Five different objects were used to test the robotic hand, three objects for grasping task, and two objects for pinching task. For object 1 as an example of robotic handwork during the grasping task. In the control process, the predefined position for each object was determined; therefore, the reference position of object 1 recorded using a multi-turn potentiometer was then used as a reference point for the later control process.

The control process was to control the main DC motor motion, which accelerate the hand fingers to grasping object securely and safely. During that process, the multi-turn potentiometer output voltage signal was recorded to determine the travelled distance by the hand and the error for each step until the hand task was accomplished. Before starting the pinching task, the length of the coupler link of the second four-bar linkages for each finger was reduced using DC motor mounted on each finger. The process during the pinching task is the same as that during the grasping task.

6. Results and Discussion

6.1. Performance of the hand

The proposed self-adaptive robotic hand can grasp and pinch different objects. Figure 10 illustrates five examples of grasping and pinching tasks using the robotic hand prototype.

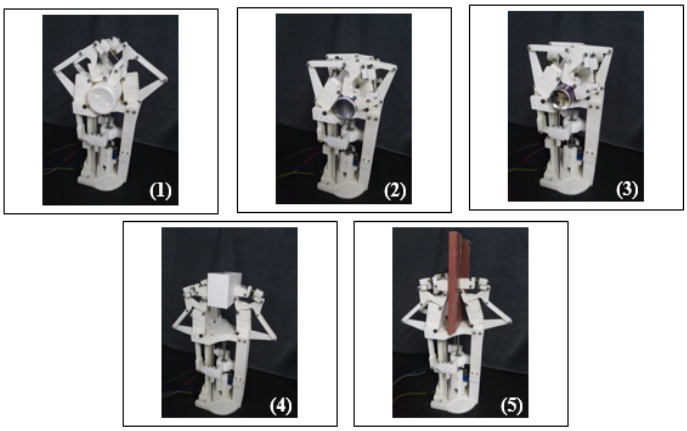

Fig. 10. Robotic hand grasping and pinching different objects.

6.2. PID controller results

The PID controller was implemented in this study to provide a proper control signal to drive the main DC motor of the Robotic hand. The output signals of the control system represent the potentiometers measurement. Figures. 11-20 show the responses of the implemented control system for the hand during a typical cylindrical grasp with various objects, as listed in Table 1.

Table 1. The used objects for grasping and pinching activities.

Object	Dimensions	Unit
Object 1	Dia.=75	mm
Object 2	Dia.=60	mm
Object 3	Dia.=50	mm
Object 4	(40×60×110)	mm^3
Object 5	(15×150×135)	mm^3

As shown in Fig. 11, the displacement for grasping the object 1 is 36 mm. The motor voltage was applied for grasping the object 1 is shown in Fig. 12, and the time is taken to implement this operation is 2.6 seconds. From Fig. 13, it can be seen that the displacement for grasping the cylindrical object 2 of a 60 mm diameter is 49 mm, while the motor takes 3.2 seconds for grasping the object, as shown in Fig. 14 compared to the previous case object 1, the slider travels more linear displacement to enable the hand envelopes the object. It can be seen from Fig. 15, the displacement for grasping object 3 with 50 mm diameter is 56 mm.

It is found that the motor takes 3 seconds to grasp in the object stably, as illustrated in Fig. 16. From the plotted result Fig. 17, the linear displacement of the robot hand for pinching the object 4 of thickness 17 mm is 19 mm. The control effort of the motor is illustrated in Fig. 18, and the time needed to pinch the object 4 stably is 1 second. The linear displacement of the robotic hand and the control signals to drive the DC motor of the system for pinching the object 5 are illustrated in Figs. 19 and 20, respectively. It can be seen that the displacement is 11mm ,and the time required for pinching the object is 8 seconds.

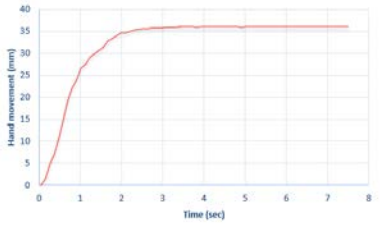

Fig. 11. Potentiometer reading of hand movement during grasping object 1.

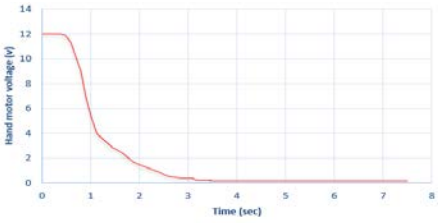

Fig. 12. hand motor behaviour through grasping the object 1.

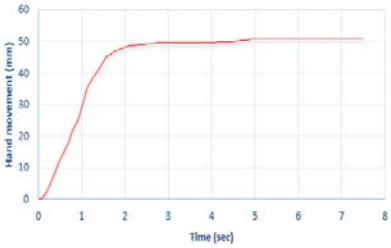

Fig. 13. Potentiometer reading of hand movement during grasping object 2.

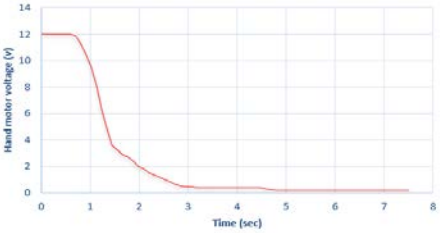

Fig. 14. Hand motor behaviour through grasping object 2.

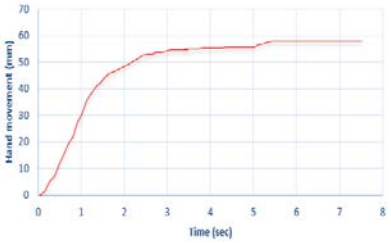

Fig. 15. Potentiometer reading of hand movement during grasping object 3.

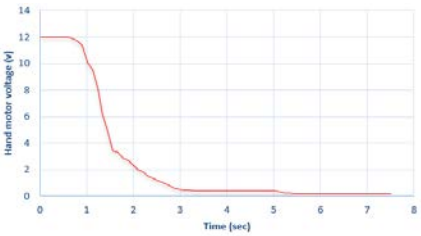

Fig. 16. Hand motor behaviour through grasping object 3.

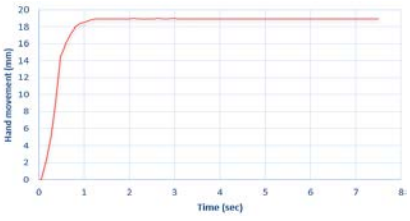

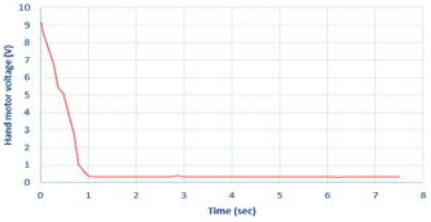

Fig. 17. Potentiometer reading of hand movement during pinching object 4.

Fig. 18. Hand motor behaviour through pinching object 4.

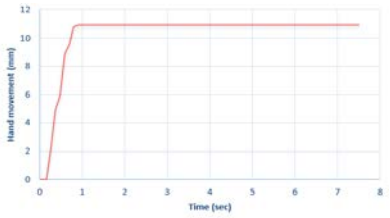

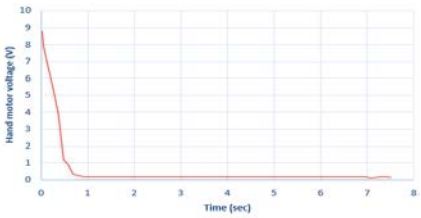

Fig. 19. Potentiometer reading of hand movement during pinching object 5.

Fig. 20. Hand motor behaviour through pinching object 5.

7. Conclusions

The proposed underactuated multi-finger linkage robotic hand was designed and constructed; this resembles the human finger for performing both grasping and pinching tasks. The evaluation of the hand prototype was strictly experimental for both configurations, where the experiment results manifested that the designed underactuated multi-finger robotic hand could grasp and pinch various objects. A single DC motor was used to accelerate the three-fingers hand to perform grasping configuration, while another DC motor with screw mounted on each finger to adjust the finger length to perform both configurations. The main conclusions are listed below:

- The transmission ratio of three phalanges four-bar linkages was formulated; the finger geometrical parameters mainly effected the transmission ratio for a specified range of the finger angles which could be maximized to increase the grasping forces.
- This mechanism has been satisfied the requirements of safe design and simple control.
- The study of the position control of the robotic hand with self-adaptive grasping and pinching is presented in this study. The position tracking for the multi-turn potentiometer under the PID controller was satisfactory. The results show that the PID control was efficacious in controlling the power screw movement and completed the required task successfully.
- The time to achieve a firm and secure grasp for both configurations take less than 8 seconds.

Nomenclatures

A	The link of transmission mechanism, mm
a_1	The 1st link length of the 1st four-bar linkage, mm
a_2	The 1st link length of the 2nd four bar-linkage, mm
B	The link which is connecting between the transmission mechanism and the input link of each finger, mm

b_1	The 2nd link length of the 1st four-bar linkage, mm
$b2$	The 2nd link length of the 2nd four-bar linkage, mm
$c1$	The 3rd link length of the 1st four-bar linkage, mm
$c2$	The 3rd link length of the 2nd four-bar linkage, mm
F_a	The transmitted actuator force to the robotic hand, N
K_i	Integral constant gain.
K_d	Derivative constant gain.
K_p	Proportional constant gain.
L	Potentiometer linear distance, mm
l_1	Proximal phalanx length, mm
l_2	Middle phalanx length, mm
l_3	Distal phalanx length, mm
R	The transmission ratio.
r_p	Diagonal of the four-bar linkage, mm
T_1	The applied torque to the proximal phalanx, N. m
T_2	The applied torque to the distal phalanx, N. m
t	Instantaneous time, s
$u(t)$	output voltage signal of the control system, V
Greek Symbols	
γ_1	The angle of the 1st ternary solid link, deg.
γ_2	The angle of the 2nd ternary solid link, deg.
γ_3	The angle of the 3rd ternary solid link, deg.
θ_a	The input angle from actuator to the finger, deg.
θ_1	The angle between the 1st phalanx and the horizontal axis, deg.
θ_2	The angle between the 1st phalanx and the 2nd phalanx and the horizontal axis, deg.
θ_3	The angle between the 2nd phalanx and the 3rd phalanx and the horizontal axis, deg.
θ_{13}	The angle of the 3rd ternary link and the horizontal axis, deg.
θ_{41}	The angle of 4th link of the 1st four-bar linkage with the horizontal axis, deg.
θ_{31}	The angle of 1st link of the 3rd four-bar linkage with the horizontal axis, deg.
θ_{22}	The angle of 2nd link of the 2nd four-bar linkage with the horizontal axis, deg.
τ	The variable of integration, its value from (0) to the instantaneous time (t), s
Ψ	The angle between the copular link and the output link in the 1st four-bar linkage, deg.
Ψ_1	The angle between the copular link and the output link in the 2nd four-bar linkage, deg.
ω_1	Angular velocity of the proximal phalanx, rad/s
ω_2	Angular velocity of the distal phalanx, rad/s
$\omega_{42} = \dot{\theta}_{42}$	Angular velocity of the 4th link of the 2nd four-bar linkage, rad/s
$\omega_{41} = \dot{\theta}_{41}$	Angular velocity of the 4th link of the 1st four-bar linkage, rad/s

$\omega_{22} = \dot{\theta}_{22}$	Angular velocity of the 2nd link of the 2nd four-bar linkage, rad/s

Abbreviations

DOF	Degree of freedom.
PLA	Polylactic acid or polylactide.
PID	Proportional, integral, derivative controller.

References

1. Birglen, L.; Laliberté, T.; and Gosselin, C. (2008). *Underactuation between the fingers*. Berlin: Springer Tracts in Advance Robotic.
2. Rossini, P.M.; Micera, S.; Benvenuto, A.; Carpaneto, J.; Cavallo, G.; Citi, L.; Cipriani, C.; Guglielmelli, E.; Denaro, L.; Denaro, V.; Di Pino, G.; Ferreri, F.; Hoffmann, K.P.; Raspopovic, S.; Rigosa, J.; Rossini, L.; Tombini, M.; and Dario, P. (2010). Double nerve intraneural interface implant on a human amputee for robotic hand control. *Clinical Neurophysiology*, 121(5), 777-783.
3. Ting, Z.; Wang, X.Q.; Jiang, L.; Wu, X.; Feng, W.; Zhou, D.; and Liu, H. (2016). Biomechatronic design and control of an anthropomorphic artificial hand for prosthetic applications. *Robotica*, 34(10), 2291-2308.
4. Ozawa, R.; Hashirii, K.; Yoshimura, Y.; Moriya, M.; and Kobayashi, H. (2014). Design and control of a three-fingered tendon-driven robotic hand with active and passive tendons. *Autonomous Robots*, 36(1-2), 67-78.
5. Tong, K.Y.; Ho, S.K.; Pang, P.M.K.; Hu, X.L.; Tam, W.K.; Fung, K.L.; Wei, X.J.; Chen, P.N.; and Chen, M. (2010). An intention driven hand functions task training robotic system. *Proceedings of Annual International Conference of the IEEE Engineering in Medicine and Biology Society*. Buenos Aires, Argentina, 3406-3409.
6. Meijneke, C.; Kragten, G.A.; and Wisse, M. (2011). Design and performance assessment of an underactuated hand for industrial applications. *Mechanical Science*, 2(1), 9-15.
7. Roa, M.A.; Argus, M.J.; Leidner, D.; Borst, C.; and Hirzinger, G. (2012). Power grasp planning for anthropomorphic robot hands. *Proceedings of IEEE International Conference on Robotics and Automation.* Saint Paul, USA, 563-569.
8. Atzori, M.; Gijsberts, A.; Castellini, C.; Caputo, B.; Hager, A.; Elsig, S.; Giatsidis, G.; Bassetto, F.; and Müller, H. (2014). Electromyography data for non- invasive naturally-controlled robotic hand prostheses. *Scientific. Data*, 1(1), 1-13.
9. Marcenko, O. (2018). *Design and development of an anthropomorphic metamorphic robotic hand*. M.Sc. Dissertation. School of Computing, Science and Engineering, University of Salford, Manchester, United Kingdom.
10. Licheng, W.; Yanxuan, K.; and Xiali, L. (2016). A fully rotational joint underactuated finger mechanism and its kinematics analysis. *International Journal of Advanced Robotic Systems*, 13(5), 1-9.
11. Ha, X.V.; and Nguyen, D.K. (2016). A General contact force analysis of an under-actuated finger in robot hand grasping. *International Journal of Advanced Robotic Systems*, 13(1), 1-17.

12. Carbone, G.; Rossi, C.; and Savino, S. (2015). Performance comparison between FEDERICA hand and LARM hand. *International Journal of Advanced Robotic Systems*, 12(7), 1-12.
13. Zappatore, G.; Reina, G.; and Messina, A. (2019). A toolbox for the analysis of the grasp stability of underactuated fingers. *Robotics*, 8(2), 1-16.
14. Kragten, G.; Helm, F.; Herder, J. (2011). *Underactuated Robotic Hands for Grasping in Warehouses*. London: Springer International Publishing.
15. Mata, A.S.; Torras, A.B.; Carrillo, J.A.C.; Juanco, F.E.; Fernández, A.J.G.; Martínez, F.N.; and Fernández, A.O. (2016). F*undamentals of Machine Theory and Mechanisms*. Switzerland: Springer International Publishing.
16. Jabbar, M.A.; Bakhy, S.H.; and Flaieh, E.H. (2019). A new multi-objective algorithm for underactuated robotic finger during grasping and pinching assignments. *Proceeding of the 3rd International IOP Conference on Engineering Sciences.* Kerbala, Iraq, 1-28.
17. Ogata, K. (2010). *Modern control engineering* (5th ed.). New Jersey: Prentice Hall.

Appendix A

The Dimensions of The Robotic Hand Palm and Base

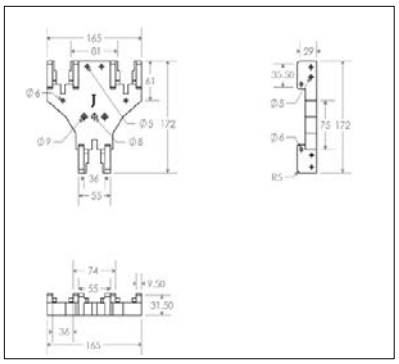

Fig. A-1. Dimensions of the robotic hand palm in mm.

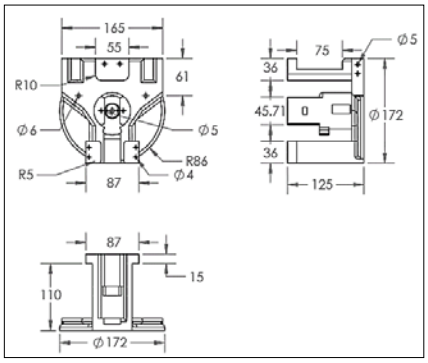

Fig. A-2. Sections of the robotic hand base (dimensions in mm).